eng

MDPI

Article

Mechanical Characterization of Cemented Paste Backfill

Andrew Pan * and Murray Grabinsky

Department of Civil and Mineral Engineering, University of Toronto, 35 St. George Street, Toronto, ON M5S 1A4, Canada
* Correspondence: andrew.pan@mail.utoronto.ca

Abstract: Mechanical characterization is important to the design and analysis of cemented paste backfill (CPB) structures. Unconfined compressive strength (UCS) tests have been widely used owing to their relative simplicity to characterize a material's response to unconfined compressive loading. However, the UCS represents a single strength parameter and does not fully describe the material's strength (or failure) envelope. In this study, we analyzed UCS tests with direct shear and uniaxial tensile strength tests conducted on the same CPB materials to provide mechanical characterization of CPB under a more complete range of loading conditions. The results demonstrate the Mohr–Coulomb failure envelope provides a consistent description of strengths arising from the three different test methods. Furthermore, a better estimate of the tensile strength is UCS/4, which is considerably higher than the conventional assumption that the tensile strength is equal to USC/10 or UCS/12. This has a significant impact on the assessed required strengths particularly for undercut designs using Mitchell's sill mat analysis method and suggests that in future the conventional UCS tests should be complemented with direct tension and direct shear tests to improve underground designs using CPB.

Keywords: unconfined compressive strength; cemented paste backfill; shear strength; tensile strength; Mohr–Coulomb envelope

Citation: Pan, A.; Grabinsky, M. Mechanical Characterization of Cemented Paste Backfill. *Eng* **2023**, *4*, 738–747. https://doi.org/10.3390/eng4010044

Academic Editors: George Z. Papageorgiou and F. Pacheco Torgal

Received: 25 December 2022
Revised: 27 January 2023
Accepted: 24 February 2023
Published: 26 February 2023

1. Introduction

Cemented paste backfill (CPB) plays an increasingly important role in underground mines due to its rapid delivery rate, reduced rehabilitation costs, safe disposal of mine wastes, and environmental benefits [1,2]. CPB is a composite backfill technique used in hard rock mining, in which mine tailings are mixed with hydraulic binder and placed underground to form a self-support structure [1,2]. The mixture designs are based on regional ground conditions, tailing behaviors, and operational requirements [1,3–5]. The stability of CPB structures is of great concern in engineering applications that are integral to ground stability [6,7].

CPB enables operations to implement sequential extraction techniques that eliminate ore pillars and enable greater recovery yield [8,9]. It also supports operations in poor ground conditions [8,9]. CPB has been demonstrated as an effective technique to address rock bursts in both Canada and the US, including Red Lake Mine in Ontario and Lucky Friday Mine in Idaho [8,10]. CPB reduces tailing surface disposal volumes, surface subsidence, and reduces risks associated with above-ground facilities which reduces rehabilitation costs and associated environmental impacts [2,11]. CPB has become an area of focus for both academic research and industry interest [1,2]. Research has enhanced CPB properties such as density and strength through mix design, admixtures, and optimized water contents [1,2,7,11].

Mechanical characterization is crucial in the design of CPB structures, which is of practical importance in mine safety [6,12]. A significant number of studies have focused on the mechanical properties of CPB which include direct shear, triaxial, and tensile tests [7,12–15]. UCS remains one of the most widely used parameters in the design of CPB due to its simplicity and historical practice [6,12]. In 1982, Mitchell et al. (1982) performed physical

model studies and field tests that led to the Mitchell Analytical Solution for Sidewall Stability [6,12]. In the Mitchell's Analytical Solution, the backfills were conducted with sidewall exposure, the observed failure was interpreted by a wedge failure mechanism based on the UCS, which gained wide acceptance and is still practiced in many operations [1,2,9]. In his subsequent publication, Mitchell (1991) developed a sill mat design for undercutting [16]. His design has been refined by several researchers and adopted in numerous operations [5,10,17]. However, the analysis method is based on tensile strength, and this is then converted to a UCS using the common assumption that the tensile strength = UCS/10 or UCS/12 [2]. This assumption should be challenged, because if the tensile strength is found to be proportionately higher, then it will have a direct impact on the mine's binder consumption, and therefore operating costs.

Although previous studies contributed to understanding the mechanical properties of CPB, there are limited studies on the relationship between the UCS, direct shear, and tensile strength [18,19]. Veenstra (2013) conducted extensive testing using the UCS and direct shear demonstrated that the strength properties of CPB followed a continuous strength envelope [18]. Veenstra (2013) suggests UCS alone is inadequate to quantify the mechanical properties of CPB, in particular the tensile strength [18]. In 2021, Pan and Grabinsky developed Castable Rectangular Dogbone Specimen and Compression to Tension Load Converter to directly quantify the tensile strength of CPB with a UCS less than 500 kPa [20]. The purpose of this work is to consider a wider range of CPB with a UCS approaching 1 MPa, and to determine if the strengths obtained using direct tension, direct shear, and unconfined compression test methods can be consistently described using the conventional Mohr–Coulomb failure criterion. If so, this will add confidence to the validity of all test results, and the resulting UCS to tensile strength ratio can then be used with greater confidence in future CPB designs.

2. Materials and Methods

The tailing samples were collected from Barrick's Williams Mine, Ontario, Canada. Normal Portland Cement (NPC) was used as the basic binding agent, reflecting mine practice. The chemical compositions of samples were analyzed with Phillips Sequential X-ray fluorescence (XRF), and particle size distributions were analyzed using a hydrometer in accordance with ASTM Standard D7928 [21–23]. Table 1 shows the chemical composition of the tailing and binder, Table 2 shows the binder minerology, and Figure 1 shows the particle size distribution of the tailing [21,23].

Table 1. The tailing and binder composition [21].

Tailing Composition	**SiO_2**	**Al_2O_3**	**CaO**	**MgO**	**K_2O**	**Na_2O**	**Fe_2O_3**	**S**	**TiO_2**	**P_2O_5**	**Ba**
Content (wt.%)	59.8	12.2	3.6	3.5	3.4	3.2	2.4	0.6	0.4	0.2	0.1
Binder composition	**CaO**	**SiO_2**	**SO_3**	**Al_2O_3**	**MgO**	**Fe_2O_3**	**K_2O**	**Na_2O**			
Content (wt.%)	64.2	20.0	4.1	3.9	3.1	3.0	0.5	0.2			

Table 2. The binder mineralogy [21,23].

Minerology	**Content (w.t. %)**
Tricalcium silicate	63
Dicalcium silicate or belite	11
Tricalcium aluminate	9
Tetracalcium aluminoferrite	7

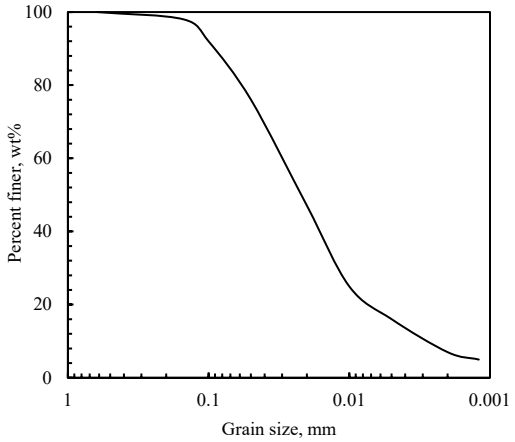

Figure 1. Mine tailing grain-size distribution [21].

Three Normal Portland Cement (NPC) binder contents of 4.2%, 6.9%, and 9.7% by percent weight of solid were selected based on mine practice. The 4.2% and 6.9% binder contents represent typical mining practice, and the 9.7% binder content represents the upper bound used for critical applications. Mine process water was used to maintain ion balance. The samples were prepared with 28% mine water content which has elevated sodium levels of 9.16 millimole per liter [21]. Table 3 shows the test configuration.

Table 3. Test configurations.

Binder Content, %	Binder Type	Curing Time, Days	Number of Trials	Number of Samples	Bulk Density, g/cm^3
4.2	100% NPC	3, 7, 14, 28	3	9	1.884
6.9	100% NPC	3, 7, 14, 28	3	9	1.897
9.7	100% NPC	3, 7, 14, 28	3	9	1.911

The samples were prepared with 4-part spilt molds as shown in Figure 2. The sample apparatus consisted of a top cap, 2 side enclosures, and a base plate. The side enclosures initially hold a small excess of material, and the top cap contains several holes so that the excess material is extruded as the top cap is attached. This method ensures the sample's ends are smooth and parallel. The specimens were 70 mm high and 35 mm in diameter, in accordance with ASTM Standard D2166 for Unconfined Compressive Strength of Cohesive Soil [24]. The specimens were sealed and cured in water to preserve the sample's water content and simulate the saturated, high relative humidity condition that is known to exist in the field based on extensive field sampling and bulk property testing [20,25,26].

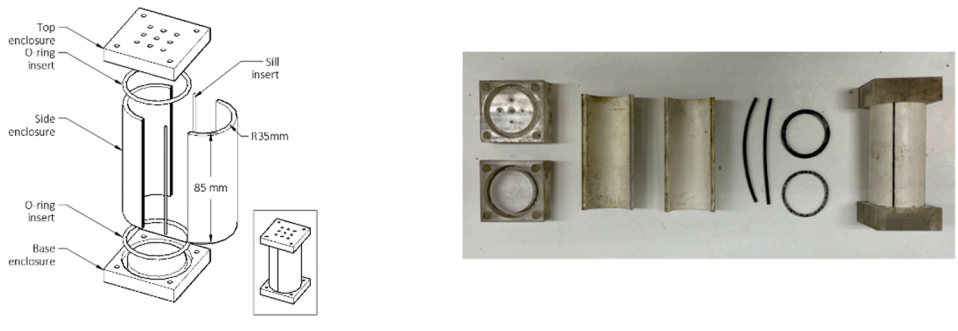

Figure 2. UCS mold assembly. (**A**) Mold schematic. (**B**) Mold photograph.

The experiments were conducted with a Wille Geotechnic Tabletop Electromechanical Consolidation Apparatus as shown in Figure 3. The test was conducted at 0.5% strain rate in accordance with ASTM Standard D2166 [24].

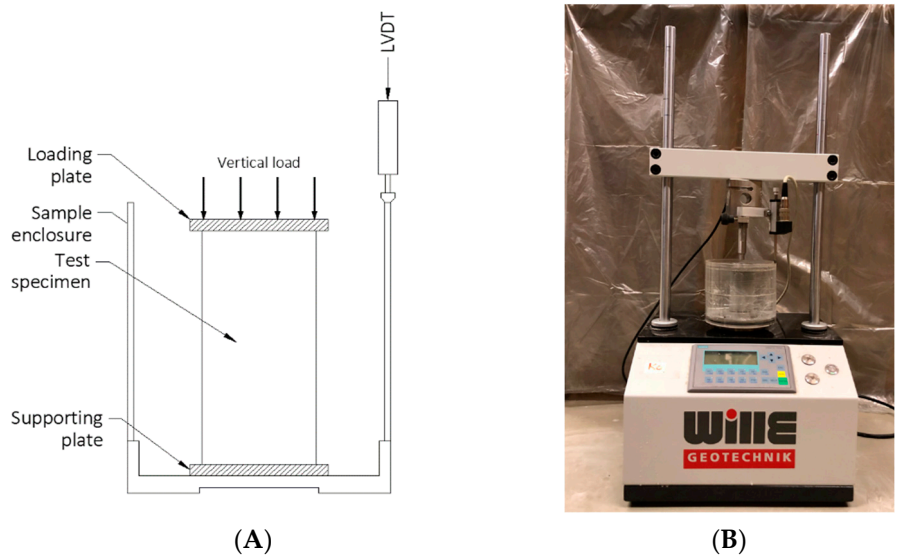

Figure 3. Experimental Setup. (**A**) Test schematic. (**B**) System photograph.

3. Results and Discussion

The effect of the curing time and binder contents on the strength and stiffness of CPB are assessed using direct shear, unconfined compression, and tensile strength test methods. Figure 4 shows the stress–strain properties follow three phases: a. an initial elastic behavior, b. yield at 0.5% strain with a plateau region and peak strength, and c. post-peak behavior from 1% onward. The yield point is consistent with direct shear, which can be attributed to the propagation of cracks generated in the pre-peak and peak regions [25].

Figure 5 shows the UCS with the cement content and curing time. The UCS increase between 3 to 28 days' curing time can be characterized by the power relationship (Equation (1)) as shown in Figure 5A.

$$P = a\ t^b \quad (1)$$

where P is the compressive strength, a is the constant coefficient, t is the curing time in days, and b is the power coefficient. The coefficient of the determination R^2 value is greater than 0.9 for all 4.2%, 6.9%, and 9.7% CPB trials. The results are consistent with a cohesion increase with direct shear [25]. The results show a more obvious trend in 9.7% CPB than those of 4.2% and 6.9%, which can be explained by the fact that higher binder hydration with time will lead to the formation of more hydration product. The trend is consistent with the shear behavior reported by Fall et al. (2007) [12].

Figure 5B shows the UCS with the binder contents. The results show the strength increase between the 4.2% to 9.7% binder contents can be characterized by the linear relationship.

$$P = a\ c_s + b, \quad (2)$$

where P is the compressive strength, a is the coefficient, c_s is the binder contents, and b is the power coefficient. The R^2 value is greater than 0.95 in all 4.2%, 6.9%, and 9.7% CPB tests. The trend is consistent with the cohesion in direct shear [27]. The trend is more obvious in the 28-day curing time than those for 3, 7, and 14 days, which could be attributed to a higher cement content resulting in a more pronounced hydration effect. The result is consistent with direct shear in which the degree of strength gain is proportional to the binder percentage in CPB with a binder content between 3 to 10 percent [6,27].

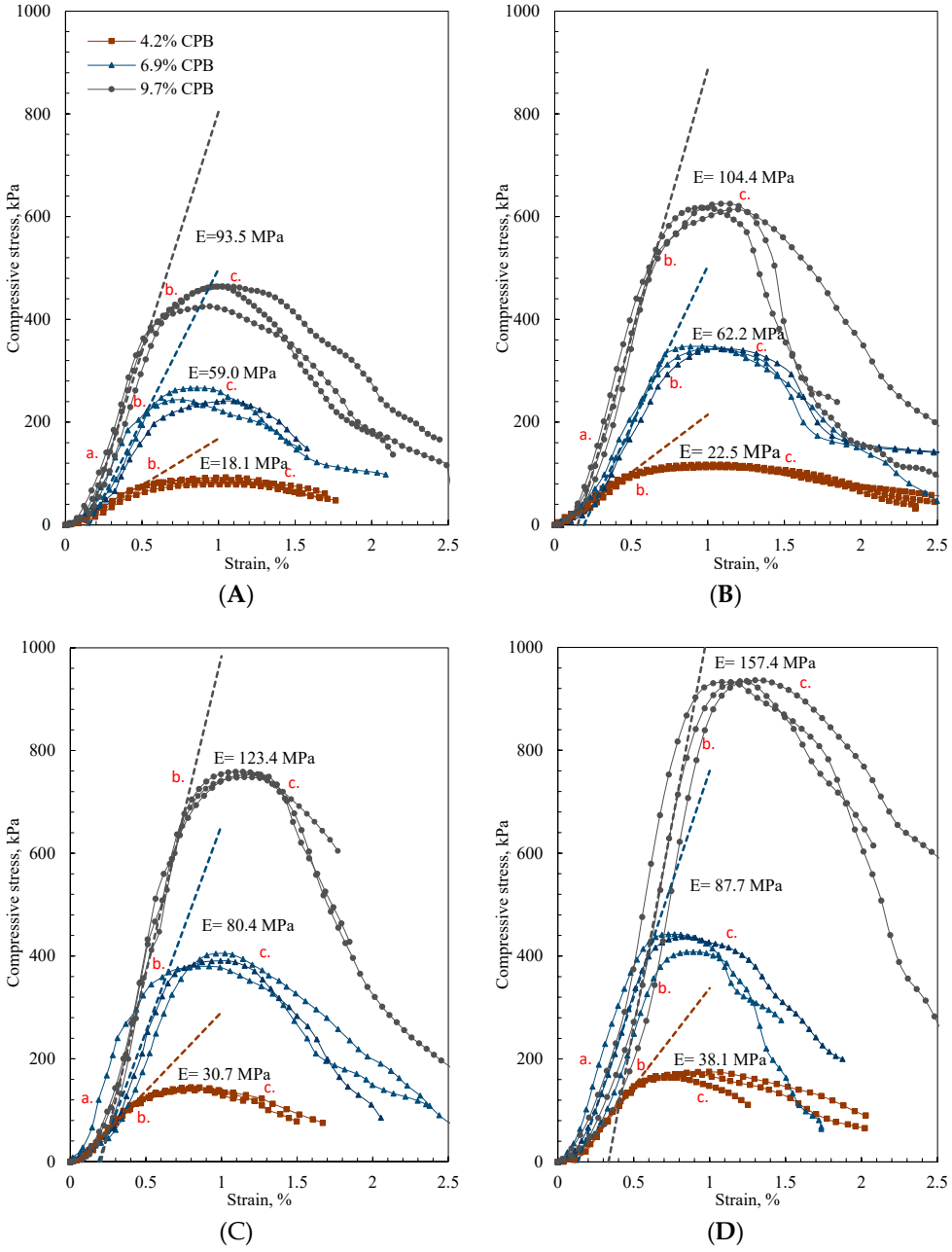

Figure 4. The stress–strain properties of UCS. (**A**) 3 Day curing interval. (**B**) 7 Day curing interval. (**C**) 14 Day curing interval. (**D**) 28 Day curing interval.

The effect of the binder content and curing time are reflected on the stress–strain properties. At lower binder contents and early curing time, the stress–strain curves show more plastic behavior. By contrast, the higher binder contents and longer curing time have a more defined response, which could be attributed to more developed cement bonds. The post-peak stress–strain response of CPB is due to accumulated energy which leads to a quick propagation of cracks in the failure zone, and subsequently, the stress decreases sharply [12]. The trend is reflected in the stiffness.

Figure 6 shows the modulus of elasticity with the curing time and cement content. The modulus of elasticity with the curing time and binder content of CPB can be empirically expressed by:

$$E = c\, t^{d}, \quad (3)$$

where E is the modulus of elasticity, c is a constant coefficient, t is the curing time in days, and d is a power coefficient. As expected, as the curing time and the binder contents increase, CPB tends to harden due to more developed cement bonds. This hardening will result in an increased stiffness. The result is consistent with the studies by Fall et al. (2007), Nasir and Fall (2008), Pan and Grabinsky (2021) [12,25,27].

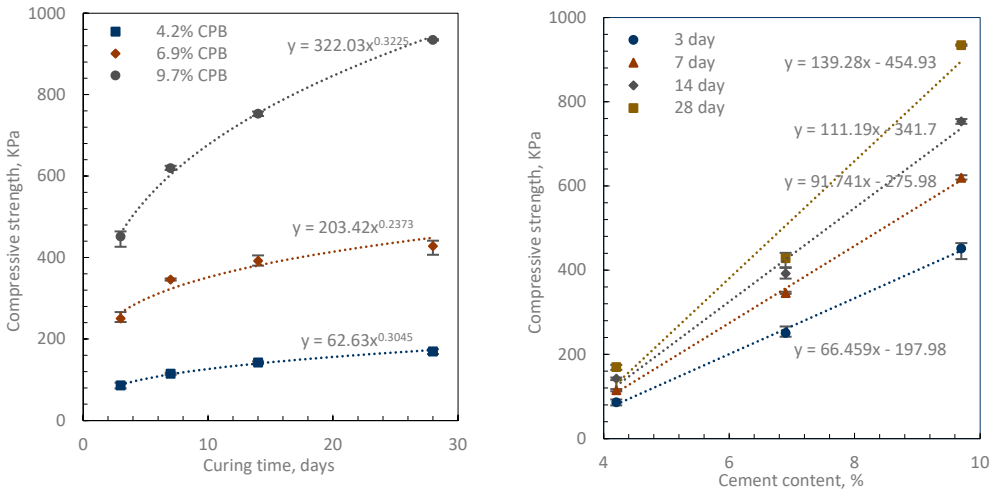

(**A**) (**B**)

Figure 5. UCS strength properties with curing time and binder content. (**A**) UCS strength with curing time, (**B**) UCS strength with binder content.

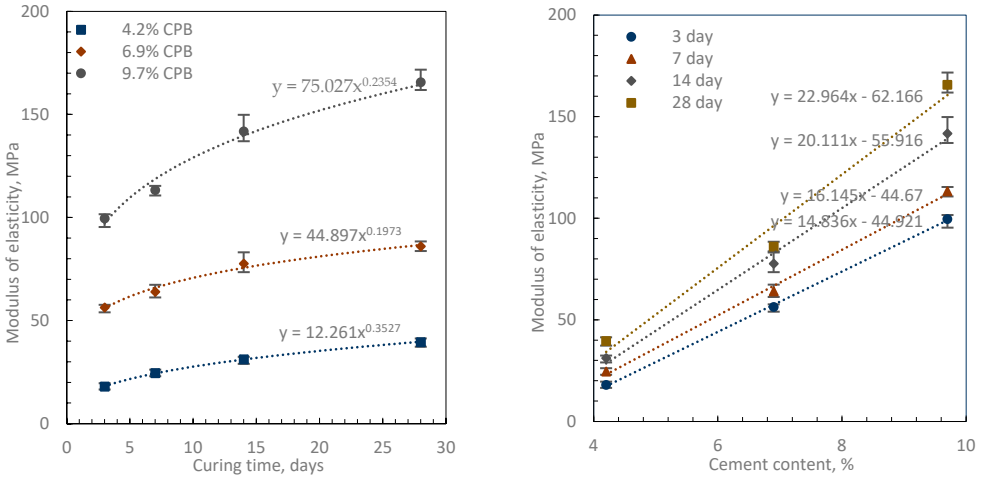

(**A**) (**B**)

Figure 6. Modulus of elasticity. (**A**) Modulus of elasticity with curing time, (**B**) modulus of elasticity with binder content.

Figure 7 shows the comparison of the UCS with the direct shear and tensile strength results in Mohr's stress space [20,25,28]. The direct shear and direct tension test results are from published testing results using the same materials [20,25]. Note that the direct shear test results are plotted in Figure 7 using markers (triangles, squares, and circles), with each marker corresponding to the normal stress at which the test was conducted, and the peak shear strength obtained in that test. The Mohr's failure circle for the UCS and tensile tests are plotted in Figure 7 for direct comparison with the linear Mohr–Coulomb failure envelope fit to the direct shear tests. The tensile strength with a cement content less than 6.7% and curing interval shorter than 3 days were not analyzed due to the softness of

the specimen [20]. The UCS and uniaxial tensile Mohr's circles are tangent to the linear strength envelope from the direct shear data, demonstrating that the Mohr–Coulomb criterion appropriately quantifies the strengths arising from all test methods. The strength behavior of CPB can be characterized by the Mohr–Coulomb envelope [29]:

$$\tau = \sigma_n \tan \phi_p + c \tag{4}$$

where τ is the shear stress, σ_n is the normal stress, ϕ_p is the angle of frictional resistance, and c is the cohesion. The shear resistance increases linearly with stresses with an R^2 value over 0.9. The strength envelope is shown to extend to uniaxial tension with 6.9% and 9.7% CPB at 7-, 14-, and 28-day curing intervals.

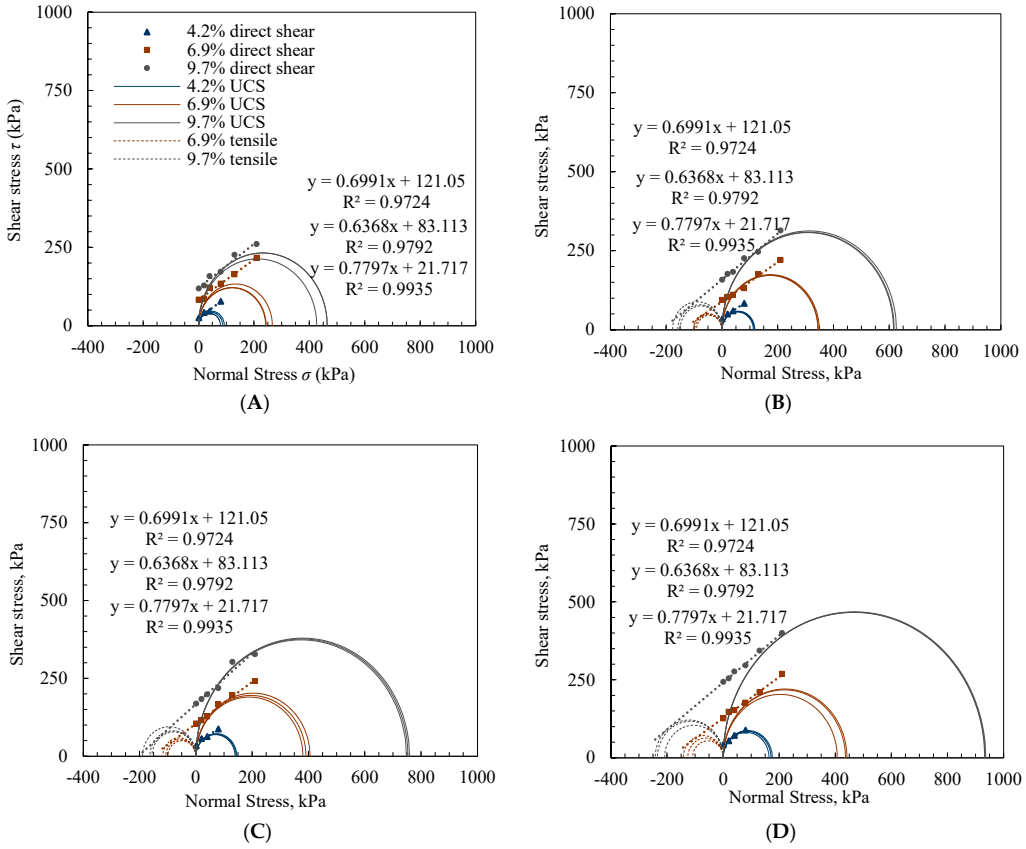

Figure 7. UCS with shear and tensile strength. (**A**) 3 Day curing interval. (**B**) 7 Day curing interval. (**C**) 14 Day curing interval. (**D**) 28 Day curing interval.

Figure 8 shows the comparison of the measured and calculated compressive and tensile strengths from the Mohr–Coulomb parameters for envelopes fit to the direct shear data. The UCS is calculated as [29]:

$$\sigma_c = 2c/\tan(45 - \varphi/2) \tag{5}$$

The tensile strength is calculated as [29]:

$$\sigma_t = 2c/\tan(45 + \varphi/2) \tag{6}$$

where σ_c is the compressive strength, σ_t is the tensile strength, c is the cohesion, and φ is the angle of frictional resistance. The calculated UCS results are consistent with the measured values in trials of the 4.2, 6.9, and 9.7%, and the back-analyzed tensile results are consistent with all measured values in the 6.9% and 9.7% test results. These results show the tensile strength is significantly greater than 1:10 or 1:12 of the UCS [16,17]. The back-analyzed

UCS strength is compatible with the experimental results in all of the 4.2%, 6.9%, and 9.7% trials shown in Figure 7. These results are valid for the strength properties obtained over the full range of the studied curing time and binder contents.

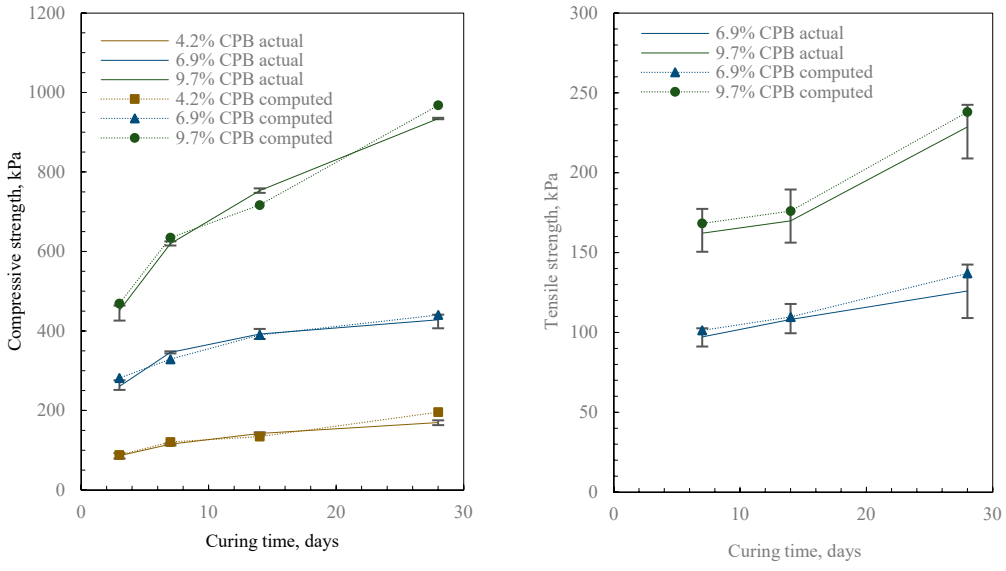

(**A**) (**B**)

Figure 8. UCS and tensile strength back-analysis. (**A**) Compressive strength with curing time. (**B**) Tensile strength with curing time.

These results illustrate the relationship between the compressive, shear, and tensile strengths. While the UCS has provided a long-standing insight into the unconfined strength properties of CPB, the UCS should be complemented with direct shear and direct tensile tests for a fuller understanding of CPB's strengths over the range of confining stresses relevant to design. Our study shows Mohr–Coulomb parameters are better at indirectly estimating the tensile strength and suggests the long-held assumption that a tensile strength of approximately 1:10 or 1:12 of the UCS is overly conservative from an economic perspective (i.e., it will over-estimate the CPB's required binder content, and therefore unnecessarily inflate backfill costs). However, it should be noted that both the Mohr–Coulomb estimation and the 1:10 to 1:12 ratios are empirical, and so the tensile strength should be quantified through direct measurement whenever possible. We recommend that mine operations integrate direct shear and direct tensile testing in the mechanical characterization program to enable more reliable data, and therefore more economic design that allows for greater efficiency.

4. Conclusions

This paper presents the results of an experimental investigation of the strength properties of CPB. The UCS behavior was assessed with direct shear and direct tensile strengths through four curing time intervals and three binder contents. The results show that Mohr–Coulomb parameters provide a better indirect determination of the tensile strength and suggest the tensile strength estimate of 1:10 or 1:12 of the UCS is overly conservative from a cost perspective. However, the Mohr–Coulomb approach also represents an empirical correlation, and so the tensile strength should be quantified through direct measurement whenever possible. Mechanical characterization is crucial to the rational design of CPB structures. Our study indicates that the current design approach for undercut CPB using Mitchell's sill mat method could be optimized through direct tensile tests combined with UCS and direct shear tests, which may provide significant operational savings and enhance wider adoption of CPB.

The study was conducted for a specific tailing stream and binder type. It should not be assumed for other tailing and binder combinations. However, it provides a baseline for mine operators and researchers to quantify their materials and optimize backfill design.

Author Contributions: Conceptualization, A.P. and M.G.; methodology, A.P.; software, A.P.; validation, A.P. and M.G.; formal analysis, A.P.; investigation, A.P.; resources, M.G.; data curation, A.P.; writing—original draft preparation, A.P.; writing—review and editing, A.P. and M.G.; visualization, A.P.; supervision, M.G.; project administration, A.P.; funding acquisition, M.G. All authors have read and agreed to the published version of the manuscript.

Funding: This study was funded in part by the National Science and Engineering Research Council (NSERC) of Canada, University of Toronto, and the industrial funding from the Barrick Gold Corporation.

Data Availability Statement: All data, models, or code that support the findings of this study are available from the corresponding author upon reasonable request.

Acknowledgments: The authors would like to provide special acknowledgement for Xiaoyu Song from Portland State University for his technical support. The authors would also like to thank William's Operation for providing tailings, binders, and process water.

Conflicts of Interest: The authors declare no conflict of interest.

References

1. Hassani, F.; Archibald, J. *Mine Backfill*; Canadian Institute of Mining, Metallurgy and Petroleum: Montreal, QC, Canada, 1998.
2. Paterson & Cooke Canada Inc. *Mine Backfill Design & Operation Course*; Patterson & Cooke: Sudbury, ON, Canada, 2019.
3. Le Roux, K.; Bawden, W.F.; Grabinsky, M.F. Field properties of cemented paste backfill at the Golden Giant mine. *Min. Technol.* **2005**, *114*, 65–80. [CrossRef]
4. Kesimal, A.; Yilmaz, E.; Ercikdi, B.; Alp, I.; Deveci, H. Effect of properties of tailings and binder on the short-and long-term strength and stability of cemented paste backfill. *Mater. Lett.* **2005**, *59*, 3703–3709. [CrossRef]
5. Raffaldi, M.J.; Seymour, J.B.; Richardson, J.; Zahl, E.; Board, E. Cemented Paste Backfill Geomechanics at a Narrow-Vein Underhand Cut-and-Fill Mine. *Rock Mech. Rock Eng.* **2019**, *52*, 4925–4940. [CrossRef] [PubMed]
6. Mitchell, R.J.; Olsen, R.S.; Smith, J.D. Model studies on cemented tailings used in mine backfill. *Can. Geotech. J.* **1982**, *19*, 14–28. [CrossRef]
7. Fall, M.; Benzaazoua, M.; Ouellet, S. Experimental characterization of the influence of tailings fineness and density on the quality of cemented paste backfill. *Miner. Eng.* **2005**, *18*, 41–44. [CrossRef]
8. Pakalnis, R.; Caceres, C.; Clapp, K.; Morin, M.; Brady, T.; Williams, T.; Blake, W.; MacLaughlin, M. Design Spans—Underhand Cut and Fill Mining. In Proceedings of the 107th Canadian Institute of Mining Annual General Meeting, Toronto, ON, Canada, 1–9 April 2005.
9. De Souza, E.; Archibald, J.F.; Dirige, A.P. Underground Backfill Practices in Canadian Mines. In Proceedings of the 6th North America Rock Mechanics Symposium (NARMS), Houston, TX, USA, 6–9 June 2004.
10. Keita, A.M.T.; Jahanbakhshzadeh, A.; Li, L. Numerical analysis of the failure mechanisms of sill mats made of cemented backfill. *Int. J. Geotech. Eng.* **2021**, *7*, 802–814. [CrossRef]
11. Skrzypkowski, K. 3D Numerical Modelling of the Application of Cemented Paste Backfill on Displacements around Strip Excavations. *Energies* **2021**, *14*, 7750. [CrossRef]
12. Fall, M.; Belem, T.; Samb, S.; Benzaazoua, M. Experimental characterization of the stress–strain behaviour of cemented paste backfill in compression. *J. Mater. Sci.* **2007**, *42*, 3914–3922. [CrossRef]
13. Tikou, B.; Benzaazoua, M.; Bussière, B. Mechanical behaviour of cemented paste backfill. In Proceedings of the 53rd Canadian Geotechnical Conference, Montreal, QC, Canada, 15–18 October 2000.
14. Jafari, M.; Shahsavari, M.; Grabinsky, M. Drained Triaxial Compressive Shear Response of Cemented Paste Backfill (CPB). *Rock Mech. Rock Eng.* **2021**, *54*, 3309–3325. [CrossRef]
15. Guo, L.; Peng, X.; Zhao, Y.; Liu, G.; Tang, G.; Pan, A. Experimental Study on Direct Tensile Properties of Cemented Paste Backfill. *Front. Mater.* **2022**, *9*, 864264. [CrossRef]
16. Mitchell, R. Sill mat evaluation using centrifuge models. *Min. Sci. Technol.* **1991**, *13*, 301–313. [CrossRef]
17. Grabinsky, M.; Jafari, M.; Pan, A. Cemented Paste Backfill (CPB) Material Properties for Undercut Analysis. *Mining* **2022**, *2*, 103–122. [CrossRef]
18. Veenstra, R.L. A Design Procedure for Determining the In Situ Stresses of Early Age Cemented Paste Backfill. Doctoral Thesis, University of Toronto, Toronto, ON, Canada, 2013.

19. Johnson, J.C.; Seymour, J.B.; Martin, L.A.; Stepan, M.; Arkoosh, A.; Emery, T. Strength and Elastic Properties of Paste Backfill at the Lucky Friday Mine, Mullan, Idaho. In Proceedings of the 49th U.S. Rock Mechanics/Geomechanics Symposium, San Francisco, CA, USA, 1 July 2015.
20. Pan, A.N.; Grabinsky, M.W.F. Tensile Strength of Cemented Paste Backfill. *Geotech. Test. J.* **2021**, *44*, 1886–1897. [CrossRef]
21. Jafari, M. Experimental Study of Physical and Mechanical Properties of a Cemented Mine Tailings. Ph.D. Thesis, University of Toronto, Toronto, ON, Canada, 2020.
22. *ASTM-D7928*; Standard Test Method for Particle-Size Distribution (Gradation) of Fine-Grained Soils Using the Sedimentation (Hydrometer) Analysis. ASTM International: West Conshohocken, PA, USA, 2017.
23. Klein, K.; Simon, D. Effect of specimen composition on the strength development in cemented paste backfill. *Can. Geotech. J.* **2016**, *43*, 310–324. [CrossRef]
24. *ASTM D2166-06*; Standard Test Method for Unconfined Compressive Strength of Cohesive Soil. ASTM International: West Conshohocken, PA, USA, 2010.
25. Pan, A.N.; Grabinsky, M.W.F.; Guo, L. Shear Properties of Cemented Paste Backfill under Low Confining Stress. *Adv. Civ. Eng.* **2021**, *2021*, 7561977. [CrossRef]
26. Thompson, B.D.; Grabinsky, M.; Veenstra, R.; Bawden, W. In situ pressures in cemented paste backfill—A review of fieldwork from three mines. In Proceedings of the 14th International Seminar on Paste and Thickened Tailings, Australian Centre for Geomechanics (Paste 2011), Perth, Australia, 5–7 April 2011; pp. 491–503. [CrossRef]
27. Nasir, O.; Fall, M. Shear behaviour of cemented pastefill-rock interfaces. *Eng. Geol.* **2008**, *101*, 146–153. [CrossRef]
28. Grabinsky, M.; Pan, A. Cemented paste backfill failure envelope at low confining stress. In Proceedings of the 13th International Symposium on Mining with Backfill, Katowice, Poland, 28 May 2021.
29. Terzaghi, K. *Theoretical Soil Mechanics*; John Wiley & Sons: Hoboken, NJ, USA, 1943.